Cascaded Channel Statistics and Target Detection Analysis for IRS-assisted ISAC employing NOMA

Harsh Raj and B. R. Manoj
Department of Electronics & Electrical Engineering, Indian Institute of Technology Guwahati, Assam, India
Emails: {h.raj, manojbr}@iitg.ac.in

***Abstract*—This paper investigates the intelligent reflecting surface (IRS)-assisted integrated sensing and communication (ISAC) framework employing a non-orthogonal multiple access (NOMA) transmission scheme. In the proposed system, an ISAC transceiver employing NOMA transmits information to the downlink near and far users in the presence of the radar target and clutters, with the IRS assisting the far user. The ISAC transceiver communicates with the users while simultaneously performing mono-static sensing to detect the target. For the presented system, a new exact channel statistic for the cascaded Rician-Rayleigh link via IRS is derived using the Laplace transform to address the central limit theorem (CLT) approximation limitation in a low channel gain scenario. Thus, it enables an accurate derivation of the closed-form analytical expression for the outage probability of the system in a high signal-to-noise ratio (SNR) regime, where the optimal phase shifts at the IRS have been employed to improve the received signal at the far user. We have shown that when random phase shifts are employed at the IRS, CLT approximation is satisfied to provide accurate outage probability in all SNR regimes. Our derived analysis thoroughly investigates considering the interference caused by sensing echoes and clutters to the communication users. Further, we have derived the probability of detection of the radar target by employing the Neyman-Pearson criterion and analyzed the receiver operating characteristics for target detection in the presence of clutters. Numerical results demonstrate the proposed analytical framework through Monte-Carlo simulations for various system parameters, and comparative performance analysis reveals that the NOMA-assisted ISAC outperforms orthogonal multiple-access systems.**

***Index Terms*—Central limit theorem, intelligent reflecting surface, integrated sensing and communication, Laplace transform, non-orthogonal multiple access, and probability of detection.**

I. Introduction

The rapid growth of the Internet of Things (IoT), vehicle-to-everything communications, and connected autonomous systems is driving a paradigm shift in future wireless networks. Further, the overlap of wireless communication networks with radar systems causes the frequency spectrum to become increasingly congested as the electromagnetic spectrum resources are becoming limited [1]. Spectrum-sharing solutions are paramount in overcoming connected devices' profusion and efficiently utilizing radio resources. Thus, integrated sensing and communication (ISAC) is one of the potential solutions for 6G, enabling spectrum sharing between radar and communication [2]. ISAC aims to support smart connectivity for everything, where IoT devices gain environmental awareness, facilitate inter-device communication, and enhance quality-of-service for next-generation wireless networks. In ISAC networks, communication users (CUs) can leverage both line-of-sight (LOS) and non-line-of-sight (NLOS) paths to enhance performance by increasing degrees of freedom (DoF). In contrast, radar sensing primarily relies on LOS, treating NLOS as interference [3]. Intelligent reflecting surfaces (IRS) address this issue by introducing controllable phase shifts in the wireless signals to create a virtual LOS. The phase-shifting capability of IRS has been explored in ISAC systems to enhance the performance of both sensing and communication functionalities [4]. Although integrating communication and sensing functions is promising for 6G, achieving the balance between both functionalities is challenging due to potential interference from hardware limitations and shared radio resources. The non-orthogonal multiple access (NOMA) technique has emerged as a potential candidate that enhances spectral efficiency while managing interference and resource allocation, inspiring the exploration of NOMA in ISAC systems [5], [6]. NOMA allows multiple users to share the same resource blocks utilizing superposition coding at the transmitter and successive interference cancellation (SIC) at the user's receiver [6]. An ISAC framework with the NOMA technique was introduced in [7] to demonstrate the trade-off between communication and sensing performance. In [8], the IRS-assisted ISAC framework is presented to create virtual LOS paths for both radar targets and CUs employing the NOMA transmission scheme. Although [5]–[8] emphasize the enhancement of sensing and communication performance, the interference caused by sensing echoes and clutter on CUs are neglected, which will cause performance degradation.

In our work, we consider the investigation of the IRS-assisted downlink (DL) scenario by employing the NOMA scheme in the presence of interference caused by radar target sensing echoes and clutter on the CU. In the proposed system model, a new channel statistic is derived for the cascaded Rician-Rayleigh channel between the transmitter (Tx)-to-IRS-to-CU by utilizing the central limit theorem (CLT) and Laplace transform (LT)-based approaches to obtain the probability density functions (PDFs). By using the PDFs, the outage probability (OP) is derived for the considered system for random and optimal phase shifts of IRS elements. We demonstrate that

This work was supported by a Nokia University Donation.

2025 National Conference on Communications (NCC) | 979-8-3315-3601-5/25/$31.00 ©2025 IEEE | DOI: 10.1109/NCC63735.2025.10982964

979-8-3315-3601-5/25/$31.00 ©2025 IEEE

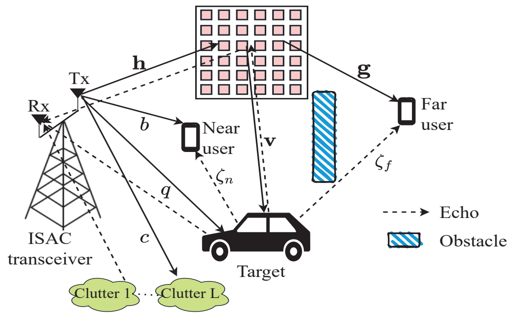

Fig. 1: IRS-assisted ISAC system employing NOMA scheme.

the CLT provides an accurate OP for random phase shifts at the IRS. However, the CLT fails to provide accurate OP in the high signal-to-noise ratio (SNR) regime for optimal phase shifts. This is because the CLT-based approach provides inaccurate channel statistics for the cascaded channel, particularly when the channel gain is low. To overcome this limitation, we derive an exact channel statistic using an LT-based approach to obtain the OP specifically in the high SNR regime. Furthermore, for the optimal phase shifts of IRS, we derive the asymptotic approximation of the OP at a high SNR to obtain the diversity order. We demonstrate that diversity order depends on IRS elements in the absence of sensing echo interference but becomes independent of IRS elements when such interference is present. We then compare the performance of the proposed system model with that of an orthogonal multiple access (OMA)-based system. Additionally, we have derived the probability of detection (PoD) and analyzed the receiver operating characteristics (ROC) by utilizing the Neyman-Pearson (NP) criterion to evaluate target sensing performance in the presence of clutter. We employ optimal phase shifts at the IRS elements to assist the far user and analyze the PoD of the target with and without IRS, providing a comprehensive investigation of the sensing performance for varying numbers of clutter.

II. System Model

An IRS-assisted ISAC system model is considered with the NOMA technique, as shown in Fig. 1. The ISAC transceiver is equipped with a single Tx and receiver (Rx). The Tx communicates directly with the near user (NU), which is a cell-centered user equipment. In contrast, the far user (FU) at the cell edge relies on the IRS for communication due to path loss caused by the obstacle. Both NU and FU have a single Rx antenna. The IRS consists of N reflecting elements with a reflection coefficient matrix denoted as $\mathbf{\Phi} = \text{diag}\left([e^{j\theta_1}, e^{j\theta_2}, \ldots, e^{j\theta_N}]\right)$, where $\theta_i \in [0, 2\pi)$ denotes the adjustable phase shift at the i-th element $i \in \{1, 2, \ldots, N\}$. The IRS is positioned in the x-y plane, consisting of $N = N_x \times N_y$ reflecting elements, where N_x and N_y denote the number of elements along the x and y axes, respectively.

A. Channel Model

The channels from Tx-to-IRS, IRS-to-FU, and Tx-to-NU are denoted as $\mathbf{h} \in \mathbb{C}^{N\times 1}$, $\mathbf{g} \in \mathbb{C}^{N\times 1}$, and $b \in \mathbb{C}$, respectively. We consider that the Tx-to-IRS channel, denoted as $\mathbf{h}$, follows Rician distribution as given by

$$\mathbf{h} = \sqrt{\frac{K\Omega}{1+K}}\mathbf{h}_{\text{LOS}} + \sqrt{\frac{\Omega}{1+K}}\mathbf{h}_{\text{NLOS}}\,, \tag{1}$$

where $\mathbf{h}_{\text{LOS}}$ and $\mathbf{h}_{\text{NLOS}} \sim \mathcal{CN}(\mathbf{0}, \sigma^2\mathbf{I}_N)$ represent the LOS and NLOS components of $\mathbf{h}$, respectively, with $\mathcal{CN}(\cdot,\cdot)$ denoting the complex Gaussian distribution, σ^2 is the variance, and $\mathbf{I}_N$ is the identity matrix of dimension $N \times N$. The Rician factor is denoted by K and $\Omega = \rho_0 d^{-\eta}$ represents the path loss of the Tx-to-IRS link with d being the link distance, η is the path loss exponent, and ρ_0 is the path loss at a reference distance d_0. The antenna array response of the IRS is modeled as $\mathbf{h}_{\text{LOS}} = \mathbf{a}_{\text{IRS}}(\phi_a, \phi_e)$ given by

$$\mathbf{a}_{\text{IRS}}(\phi_a, \phi_e) = \Big[1, \ldots, e^{-j2\pi\frac{\delta}{\lambda}(n_x \sin\phi_e \cos\phi_a + n_y \cos\phi_e)}, \ldots, e^{-j2\pi\frac{\delta}{\lambda}((N_x-1)\sin\phi_e\cos\phi_a + (N_y-1)\cos\phi_e)}\Big]^{\mathrm{T}}, \tag{2}$$

where $\phi_a \in (0, 2\pi)$ and $\phi_e \in (0, 2\pi)$ are the azimuth and elevation angle of arrival (AoA) of signal to the IRS, respectively, $0 \le n_x \le N_x - 1$, $0 \le n_y \le N_y - 1$, λ is the wavelength, and δ is the spacing between reflecting elements. The distribution of the i-th element of $\mathbf{h}$ can be written as

$$h_i \sim \mathcal{N}\left(\sqrt{\frac{K\Omega}{1+K}}\Re\{h_{i,\text{LOS}}\}, \frac{\Omega}{2(1+K)}\right) + j\mathcal{N}\left(\sqrt{\frac{K\Omega}{1+K}}\Im(h_{i,\text{LOS}}), \frac{\Omega}{2(1+K)}\right),$$

where $h_{i,\text{LOS}}$ represents the i-th component of $\mathbf{h}_{\text{LOS}}$, and $\Re\{\cdot\}$ and $\Im\{\cdot\}$ denote the real and imaginary parts, respectively. The IRS-to-FU link experiences small-scale fading, modeled as Rayleigh faded channel, $\mathbf{g} \sim \mathcal{CN}(\mathbf{0}, \sigma_f^2\mathbf{I}_N)$, where σ_f^2 denotes the variance. We consider an NLOS link from Tx-to-NU, which follows Rayleigh fading, denoted by $b \sim \mathcal{CN}(0, \sigma_n^2)$, where σ_n^2 represents the variance. Furthermore, we consider a static target in the presence of clutter. The direct channel from Tx-to-target, denoted by q, is modeled as a Rician distribution as $q \sim \mathcal{CN}(\mu_q, \sigma_q^2)$, where μ_q is the mean and σ_q^2 is the variance. The IRS-to-target channel denoted by $\mathbf{v} \in \mathbb{C}^{N\times 1}$ is assumed to follow Rayleigh fading as $\mathbf{v} \sim \mathcal{CN}(\mathbf{0}, \sigma_v^2\mathbf{I}_N)$, where σ_v^2 is the variance. We further assume that there are L clutters present in the environment, which can be modeled as $c = \sum_{l=1}^{L}\chi_l u_{tl} u_{rl}$, $l \in \{1, 2, \ldots, L\}$, where $\chi_l \sim \mathcal{CN}(0, \sigma_\chi^2)$, $\forall\, l \in \{1, 2, \ldots, L\}$, denotes the radar cross section (RCS) of the l-th clutter, u_{tl} and u_{rl} denote the channel from the Tx to l-th clutter and the channel from the l-th clutter to Rx, respectively. We consider $u_{tl} = u_{rl} = u_l$ due to the channel reciprocity, where $u_l \sim \mathcal{CN}(0, \sigma_u^2)$, $\forall\, l \in \{1, 2, \ldots, L\}$.

B. Signal Model

The superposition-coded signal is transmitted by the Tx to the CUs in the DL scenario while simultaneously having the ability to perform mono-static sensing at the ISAC transceiver. Our work primarily emphasizes communication performance in the presence of interfering sensing echoes from the target and clutter that impact both the NU and FU, while the ISAC transceiver performs mono-static sensing of the radar target. The interference associated with the reflection of the echo from the target and clutter on the NU and FU is given by ζ_n and ζ_f, respectively, where $\zeta_i \sim \mathcal{CN}(0,\sigma_{\zeta_i}^2)$, $i \in \{n,f\}$. The transmitted communication signal, denoted by x, is given as $x = \sqrt{\alpha_n P}x_n + \sqrt{\alpha_f P}x_f$, where α_n and α_f represent the power allocation coefficients for the NU and FU, respectively, with $\alpha_f = 1-\alpha_n$. Further, x_n and x_f represent the signals transmitted to NU and FU, respectively, with unit power, i.e., $\mathbb{E}[|x_n|^2] = \mathbb{E}[|x_f|^2] = 1$. The total available power at the Tx is P. We assume a fixed power allocation scheme with $\alpha_n < \alpha_f$ [9] to ensure user fairness. The received signals at the NU and FU, respectively, are expressed as

$$y_n = (b+\zeta_n)\,x + n_1 \text{ and } y_f = (\mathbf{g}^H\mathbf{\Phi}\mathbf{h} + \zeta_f)\,x + n_2\,, \quad (3)$$

where $n_1 \sim \mathcal{CN}(0,\sigma_{n_1}^2)$ and $n_2 \sim \mathcal{CN}(0,\sigma_{n_2}^2)$ denote the additive white Gaussian noise (AWGN) at the NU and FU, respectively. The transmit SNR is defined as $\mathrm{SNR} = P/\sigma_{n_j}^2$, $j=\{1,2\}$.

The echo from the radar target in the presence of clutter, received at the Rx (y_r) of the ISAC transceiver, can be expressed as

$$y_r = h_t x + cx + n_r\,, \quad (4)$$

where $n_r \sim \mathcal{CN}(0,\sigma_r^2)$ with σ_r^2 is the variance and h_t is the effective end-to-end channel from Tx-to-Rx which includes: (a) Tx-to-IRS-to-target-to-IRS-to-Rx, (b) Tx-to-target-to-Rx, (c) Tx-to-IRS-to-target-to-Rx, and (d) Tx-to-target-to-IRS-to-Rx. Thus, h_t can be written as

$$\begin{aligned} h_t = &\underbrace{\epsilon_1(\mathbf{h}^H\mathbf{\Phi}\mathbf{v})(\mathbf{h}^H\mathbf{\Phi}\mathbf{v})}_{\text{Echo via IRS}} + \underbrace{\epsilon_2\, qq}_{\text{Direct echo}} \\ &+ \underbrace{\epsilon_3\left(q(\mathbf{h}^H\mathbf{\Phi}\mathbf{v}) + (\mathbf{h}^H\mathbf{\Phi}\mathbf{v})q\right)}_{\text{Combined echo via direct and IRS}}, \end{aligned} \quad (5)$$

where $\epsilon_j \sim \mathcal{CN}(0,\sigma_{\epsilon_j}^2)$, $j \in \{1,2,3\}$, denotes the RCS of the target following the Swerling-I model [10]. We consider multiple RCS coefficients to account for the fact that the target reflects echoes from different surface areas depending on the incoming signals from the Tx and the IRS. We use ϵ_3 twice because the RCS remains the same during the signal propagation in both the Tx-to-target-to-IRS-Rx and the Tx-to-IRS-to-target-to-Rx paths. Moreover, due to channel reciprocity, the channel of the reflected echo signal from the target is assumed to be the same as that of the incoming signal to the target.

C. Signal-to-Interference-Plus-Noise Ratios

Based on the NOMA principle, only signal x_f is decoded at the FU, treating the NU signal as interference. The signal-to-interference-plus-noise ratio (SINR) at the FU is expressed as

$$\Gamma_f = \frac{\alpha_f P|\mathbf{g}^H\mathbf{\Phi}\mathbf{h}|^2}{\alpha_n P|\mathbf{g}^H\mathbf{\Phi}\mathbf{h}|^2 + \sigma_{\zeta_f}^2 P + \sigma_{n_2}^2}\,. \quad (6)$$

At the NU, the FU signal x_f is first decoded and the corresponding SINR is given by

$$\Gamma_n^f = \frac{\alpha_f P|b|^2}{\alpha_n P|b|^2 + \sigma_{\zeta_n}^2 P + \sigma_{n_1}^2}\,, \quad (7)$$

Subsequently, the NU performs SIC to decode its signal x_n. The SINR at NU when its signal is decoded can be given by

$$\Gamma_n = \frac{\alpha_n P|b|^2}{\sigma_{\zeta_n}^2 P + \sigma_{n_1}^2}\,. \quad (8)$$

III. Outage Analysis Using CLT and LT Approaches

In this section, we derive the analytical framework for the outage probability of the proposed system. Specifically, we obtain the OP for the FU and NU in the DL scenario by exploiting the random and optimal phase shifts at the IRS elements.

A. Outage of Far User

An outage event occurs at the FU when it is unable to decode its own signal, x_f, successfully. Thus, the OP for the FU can be expressed as

$$\mathbb{P}_f = \Pr(\Gamma_f \le \Lambda_f)\,, \quad (9)$$

where Λ_f denotes the threshold SINR at the FU. By substituting (6) into (9), it can be written as

$$\mathbb{P}_f = \begin{cases} \Pr(|\mathbf{g}^H\mathbf{\Phi}\mathbf{h}|^2 \le \lambda_f)\,, & \text{if } \alpha_n < \frac{\alpha_f}{\Lambda_f}\,, \\ 1\,, & \text{if } \alpha_n \ge \frac{\alpha_f}{\Lambda_f}\,, \end{cases} \quad (10)$$

where $\lambda_f = \frac{\Lambda_f(\sigma_{n_2}^2 + P\sigma_{\zeta_f}^2)}{P(\alpha_f - \alpha_n\Lambda_f)}$. The statistical distribution of the cascaded channel Tx-to-IRS-to-FU can be computed based on the nature of the reflection phase shifts of the IRS elements. The distribution of the cascaded channel $z = \mathbf{g}^H\mathbf{\Phi}\mathbf{h} = \sum_{i=1}^N g_i^* h_i e^{j\theta_i}$, where g_i and h_i denote the i-th element of $\mathbf{g}$ and $\mathbf{h}$, respectively.

Proposition 1: Assume that the reflection phase shifts of the IRS elements are randomly distributed, i.e., $\theta_i \in (0,2\pi)$, where $i \in \{1,2,\ldots,N\}$. By expanding $\sum_{i=1}^N g_i^* h_i e^{j\theta_i}$ and applying the CLT, the cascaded channel z follows a complex Gaussian distribution with mean zero and variance $\sigma_z^2 = \left(\frac{N\Omega\sigma_f^2}{1+K}\right)(\sigma^2 + K|h_{i,\mathrm{LOS}}|^2)$. Furthermore, $|z|^2$ follows a central chi-square distribution with 2 DoF. Thus, the OP for the FU in the case of random phase shifts of IRS can be expressed as

$$\Pr(|z|^2 \le \lambda_f) = 1 - \exp\left(-\frac{\lambda_f}{\sigma_z^2}\right). \quad (11)$$

Proposition 2: Assume that the reflection phase shifts of the IRS elements are optimized for the FU, i.e., the optimal phase shift of the i-th IRS element for a single-input single-output system is given by $\theta_i = -(\angle g_i^* + \angle h_i)$ [11], where $i \in \{1,2,\ldots,N\}$. In (10), after substituting the optimal θ_i in $|\mathbf{g}^H\mathbf{\Phi}\mathbf{h}|^2$, we obtain

$$\mathbb{P}_f = \Pr\left(W^2 \le \lambda_f\right)\,, \quad (12)$$

where $W = \sum_{i=1}^N |g_i||h_i|$.

Lemma 1: By applying the properties of the complex Gaussian distribution, we obtain the individual mean and variance of $|g_i|$ and $|h_i|$ [12]. The means of $|g_i|$ and $|h_i|$ are given

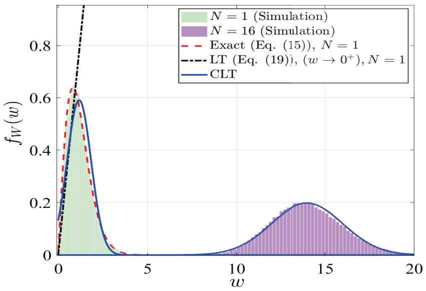

Fig. 2: CLT and LT-based PDFs of W for $N = 1$ and 16.

by $\mu_{|g_i|} = 0.5\sqrt{\sigma_f^2 \pi}$ and $\mu_{|h_i|} = \frac{1}{2}\sqrt{\frac{\pi\Omega\sigma^2}{1+K}}\xi$, respectively, where $\xi = {}_1F_1\left(-0.5, 1; \frac{a^2(1+K)}{\Omega}\right)$, ${}_1F_1(\cdot)$ is the hypergeometric function, and $a = \sqrt{\frac{K\Omega|h_{i,\mathrm{LOS}}|^2}{1+K}}$ is the non-centrality parameter of h_i. The variances of $|g_i|$ and $|h_i|$ are given as $\sigma^2_{|g_i|} = \left(2 - \frac{\pi}{2}\right)\frac{\sigma_f^2}{2}$ and $\sigma^2_{|h_i|} = \frac{\Omega\sigma^2}{1+K} + \frac{K\Omega}{1+K} - \frac{\pi\Omega\sigma^2}{4(1+K)}\xi^2$, respectively.

The mean and variance of the product of two random variables (RVs) $|g_i||h_i|$ can be obtained as $\mathbb{E}[|g_i||h_i|] = \mu_{|g_i|}\mu_{|h_i|}$ and $\mathrm{Var}[|g_i||h_i|] = \sigma^2_{|h_i|}\sigma^2_{|g_i|} + \sigma^2_{|h_i|}\mu^2_{|g_i|} + \sigma^2_{|g_i|}\mu^2_{|h_i|}$, respectively, where $\mathbb{E}[\cdot]$ and $\mathrm{Var}[\cdot]$ represent the mean and variance operators. The elements $|g_i||h_i|$ are independent and identically distributed, thus, using the CLT, the distribution of W can be approximated as $W \sim \mathcal{N}(\mu_W, \sigma_W^2)$ for a large number of reflecting elements N, where the parameters are derived as $\mu_W = \frac{N\pi\sigma_f\sigma\xi}{4}\sqrt{\frac{\Omega}{1+K}}$ and $\sigma_W^2 = \frac{N\Omega\sigma_f^2}{1+K}\left(\sigma^2 + K - \frac{\pi K\xi^2\sigma^2}{16}\right)$. Further, the distribution of W^2 can be modeled as a non-central chi-square distribution with 1 DoF. Therefore, by utilizing the CLT-based approach, the OP can be obtained as

$$\mathbb{P}_f = \Pr(|W|^2 \le \lambda_f) = 1 - Q_{\frac{1}{2}}(m_1, m_2), \quad (13)$$

where $Q_{\frac{1}{2}}(\cdot,\cdot)$ denotes the Marcum-Q function of order $\frac{1}{2}$, $m_1 = \sqrt{\mu_W}/\sigma_W$, and $m_2 = \sqrt{\lambda_f}/\sigma_W$. The OP in (13) can be further simplified as

$$\mathbb{P}_f = 1 - 0.5\left[\mathrm{erfc}\left(\frac{m_2 - m_1}{\sqrt{2}}\right) + \mathrm{erfc}\left(\frac{m_2 + m_1}{\sqrt{2}}\right)\right]. \quad (14)$$

Remark: Lemma 1 presents a computationally efficient closed-form approximation for the OP. However, the PDF of W, $f_W(w)$, obtained using the CLT-based approximation, exhibits inaccuracies near $w \to 0^+$ as demonstrated in Fig. 2. This leads to an inaccurate evaluation of the OP, particularly in the high SNR regime [13] for the DL scenario. To address this problem, we derive the exact channel statistics for channel gain near 0 by applying an LT-based approach.

Lemma 2: To apply LT, we denote $W_i = |g_i||h_i|$, representing the product of Rayleigh and Rician distributed RVs. The PDF of W_i [14, Eq. (34)] can then be obtained as

$$f_{W_i}(w) = \frac{4we^{-\varpi^2}}{\sigma_f^2\beta^2}\sum_{n=0}^{\infty}\left(\frac{1}{n!}\right)^2\left(\frac{\varpi^2}{\sigma_f^2\beta^2}\right)^n w^n K_n\left(\frac{2w}{\sigma_f\beta}\right), \quad (15)$$

where K_n represents the modified Bessel function of the second kind of n-th order, $\beta^2 = \frac{\Omega\sigma^2}{1+K}$ denotes the variance of h_i, and $\varpi = \sqrt{\frac{a^2}{\beta^2}}$. Further, Bessel-$K$ function [15, Eq. 10.30.2] can be expressed as

$$\lim_{l \to 0^+} K_n(l) \approx \frac{1}{2}\Gamma(l)\left(\frac{l}{2}\right)^{-n}, \quad n > 0. \quad (16)$$

By substituting (16) into (15) and taking LT, we get

$$\mathcal{L}_{(f^{0^+}_{W_i}(w))}(s) = \frac{2e^{-\varpi^2}}{s^2\sigma_f^2\beta^2}\sum_{n=0}^{\infty}\left(\frac{1}{n!}\right)^2\varpi^{2n}\Gamma(n). \quad (17)$$

The PDF of $W = \sum_{i=1}^{N}|g_i||h_i|$ as $w \to 0^+$ in the Laplace domain can be derived as the product of the PDFs of W_i's as

$$\mathcal{L}_{(f^{0^+}_{W}(w))}(s) = \prod_{i=1}^{N}\mathcal{L}_{(f^{0^+}_{W_i}(w))}(s) = \frac{1}{s^{2N}}\left(\frac{2e^{-\varpi^2}}{\sigma_f^2\beta^2}\sum_{n=0}^{\infty}\left(\frac{1}{n!}\right)^2\varpi^{2n}\Gamma(n)\right)^N. \quad (18)$$

After applying the inverse LT [16, (17.13.3)], we can obtain the PDF of W for $w \to 0^+$ as

$$f_W^{0^+}(w) = \frac{w^{2N-1}}{\Gamma(2N)}\left(\frac{2e^{-\varpi^2}}{\sigma_f^2\beta^2}\sum_{n=0}^{\infty}\left(\frac{1}{n!}\right)^2\varpi^{2n}\Gamma(n)\right)^N, \quad (19)$$

where $(\cdot)!$ denotes factorial. Further, the OP of FU in a high SNR regime is obtained by utilizing (19) in (12), expressed as

$$\mathbb{P}_f = F_W^{0^+}(\sqrt{\lambda_f}) = \frac{(\lambda_f)^N}{(2N)!}\left(\frac{2e^{-\varpi^2}}{\sigma_f^2\beta^2}\sum_{n=0}^{\infty}\left(\frac{1}{n!}\right)^2\varpi^{2n}\Gamma(n)\right)^N, \quad (20)$$

where $F_W^{0^+}(\cdot)$ denotes the cumulative distribution function of W for $w \to 0^+$. By substituting the value of $\lambda_f = \frac{\Lambda_f\sigma^2_{n_2}}{P(\alpha_f - \alpha_n\Lambda_f)}$ into (20), we can obtain the diversity order of the FU in the absence of interference as N. In the presence of interference, λ_f is independent of P; thus, the diversity order becomes 0.

B. Outage of Near User

The OP of the near user is given by

$$\mathbb{P}_n = 1 - \Pr(\Gamma_n^f > \Lambda_f, \Gamma_n > \Lambda_n), \quad (21)$$

where Λ_n denotes the threshold SINR for NU. After substituting (7) and (8) into (21), $\mathbb{P}_n$ is given as

$$\mathbb{P}_n = \begin{cases} 1 - \Pr(|b|^2 > \lambda_n), & \text{if } \alpha_n < \frac{\alpha_f}{\Lambda_f}, \\ 1, & \text{if } \alpha_n \ge \frac{\alpha_f}{\Lambda_f}, \end{cases} \quad (22)$$

where $\lambda_n = \max\left(\frac{\Lambda_f(\sigma^2_{n_1} + P\sigma^2_{\zeta_n})}{P(\alpha_f - \alpha_n\Lambda_f)}, \frac{\Lambda_n(\sigma^2_{n_1} + P\sigma^2_{\zeta_n})}{P\alpha_n}\right)$. Since b is a complex Gaussian RV, $|b|^2$ can be modeled as a chi-square distribution with 2 DoF. Thus, (22) becomes

$$\Pr(|b|^2 < \lambda_n) = 1 - \exp\left(-\frac{\lambda_n}{\sigma_n^2}\right). \quad (23)$$

In the absence of interference, $\sigma^2_{\zeta_n} = 0$, then the diversity order of NU becomes 1.

IV. Target Sensing: Probability of Detection

In this section, we derive the detection probability of the target for the proposed system model in the presence of clutter.

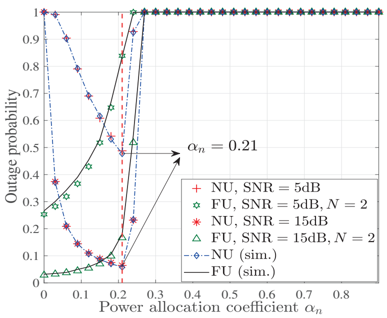

Fig. 3: OP as a function of power allocation factor α_n.

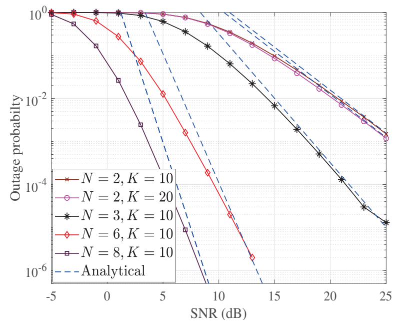

Fig. 4: OP of FU vs SNR without interference for different values of N and K.

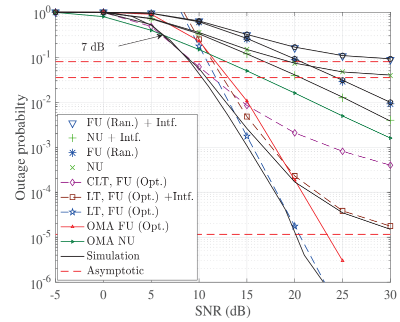

Fig. 5: OP as a function of SNR for a fixed $N = 4$.

We formulate a binary hypothesis test for the target detection by using (4), given by

$$\mathcal{H}_0 : y_r = cx + n_r \,, \tag{24}$$

$$\mathcal{H}_1 : y_r = h_t x + cx + n_r \,, \tag{25}$$

where the hypotheses $\mathcal{H}_0$ and $\mathcal{H}_1$ represent the absence and presence of the target, respectively. The reflection phase shift of the IRS element is $\theta_i = -(\angle g_i^* + \angle h_i)$, where $i \in [1, N]$ is optimized for the FU to enhance the communication performance. Since the phase shifts are aligned only for the FU, the phases of the signal from the Tx-to-IRS and IRS-to-target do not cancel each other, resulting in randomly distributed corresponding θ_i values. Further, we implement the NP lemma to derive the minimum test criteria to obtain the PoD and probability of false alarm events. The NP criterion [17] resulting in the likelihood ratio test is expressed as

$$\Delta(y_r) = \frac{f(y_r|\mathcal{H}_1)}{f(y_r|\mathcal{H}_0)} \underset{\mathcal{H}_0}{\overset{\mathcal{H}_1}{\gtrless}} \gamma_{\text{th}} \,, \tag{26}$$

where $\Delta(y_r)$ denotes the likelihood ratio, γ_{th} represents a certain threshold, $f(y_r|\mathcal{H}_1)$ and $f(y_r|\mathcal{H}_0)$ denote the conditional PDFs of the received signal when the target is present and absent, respectively. Further, when $\mathcal{H}_0$ is given, $y_r \sim \mathcal{CN}(0, \sigma_0^2)$, and when $\mathcal{H}_1$ is given, $y_r \sim \mathcal{CN}(0, \sigma_1^2)$. By applying the CLT and after some algebra, it can be shown that the variances σ_0^2 and σ_1^2 are given by

$$\begin{aligned} \sigma_0^2 &= \sigma_r^2 + 2PL\sigma_\chi^2\sigma_u^4 \,, \\ \sigma_1^2 &= P\sigma_{h_t}^2 + \sigma_r^2 + 2PL\sigma_\chi^2\sigma_u^4 \,, \end{aligned} \tag{27}$$

where

$$\sigma_{h_t}^2 = 2\sigma_{\epsilon_1}^2 \left(\frac{N\sigma_v^2 \Omega(\sigma^2 + K|h_{i,\text{LOS}}|^2)}{1+K} \right)^2 + \sigma_{\epsilon_2}^2 (2\sigma_q^4 + 4\sigma_q^2\mu_q^2 + \mu_q^4) + 4\sigma_{\epsilon_3}^2 \left(\frac{N\sigma_v^2 \Omega(\sigma^2 + K|h_{i,\text{LOS}}|^2)}{1+K} \right) (\sigma_q^2 + \mu_q^2) \,. \tag{28}$$

After substituting the conditional PDFs of $f(y_r|\mathcal{H}_1)$ and $f(y_r|\mathcal{H}_0)$ in (26), we obtain

$$\frac{\sigma_0^2}{\sigma_1^2} \exp\left(-|y_r|^2 \left\{ \frac{1}{\sigma_1^2} - \frac{1}{\sigma_0^2} \right\} \right) \underset{\mathcal{H}_0}{\overset{\mathcal{H}_1}{\gtrless}} \gamma_{\text{th}} \,. \tag{29}$$

Subsequently, taking the logarithm of (29), we obtain

$$|y_r|^2 \underset{\mathcal{H}_0}{\overset{\mathcal{H}_1}{\gtrless}} \frac{\sigma_1^2\sigma_0^2 \ln\left(\frac{\gamma_{\text{th}}\sigma_1^2}{\sigma_0^2}\right)}{\sigma_1^2 - \sigma_0^2} \,, \tag{30}$$

where $\ln(\cdot)$ is the natural logarithm. The received power $|y_r|^2$ follows the central chi-square distribution with 2 DoF. The PoD denoted by P_d and probability of false alarm denoted by P_f for the NP criterion in (26), can be respectively derived as

$$P_d = \Pr(|y_r|^2 > \widehat{\gamma}_{\text{th}}|\mathcal{H}_1) = \exp\left(-\frac{\widehat{\gamma}_{\text{th}}}{\sigma_1^2} \right), \tag{31}$$

$$P_f = \Pr(|y_r|^2 > \widehat{\gamma}_{\text{th}}|\mathcal{H}_0) = \exp\left(-\frac{\widehat{\gamma}_{\text{th}}}{\sigma_0^2} \right), \tag{32}$$

where $\widehat{\gamma}_{\text{th}} = \frac{\sigma_1^2\sigma_0^2 \ln\left(\frac{\gamma_{\text{th}}\sigma_1^2}{\sigma_0^2}\right)}{\sigma_1^2 - \sigma_0^2}$. Additionally, it is observed that the PoD is related to the probability of false alarm through the expression $P_d = P_f^{\sigma_0^2/\sigma_1^2}$.

V. Results and Discussions

In this section, we present the numerical results of the analytical OP expressions obtained for the proposed system. We consider the system parameters as: $K = 10$, $\Lambda_f = 4$, $\Lambda_n = 3$, $\sigma_{\zeta_n}^2 = \sigma_{\zeta_f}^2 = 0.009$, $\sigma_{n_1}^2 = \sigma_{n_2}^2 = 1$, $\rho_0 = 1$, $\eta = 2.3$, $\sigma^2 = 1$, $\sigma_q^2 = 2.5$, $\mu_q = 2.23$, $\sigma_{\epsilon_1}^2 = 0.9$, $\sigma_{\epsilon_2}^2 = 1$, $\sigma_{\epsilon_3}^2 = 0.8$, $\sigma_\chi^2 = 1$, $\sigma_u^2 = 0.25$, $\sigma_f^2 = 2$, $\sigma_n^2 = 5$, $\sigma_v^2 = 2$, $\sigma_r^2 = 1$, $\gamma_{\text{th}} = 10$, and $d = 2d_0$, where $d_0 = 1$ km is the reference distance between the Tx and IRS. All numerical results are thoroughly validated through Monte-Carlo simulations.

Fig. 3 illustrates the OP as a function of α_n for FU and NU. It can be observed that the NU achieves minimum outage at $\alpha_n = 0.21$ for fixed SNRs of 5 dB and 15 dB and noticed that the same value of α_n is achievable even at other SNR values. As α_n approaches 0.3, the OP saturates to 1 for FU and NU. Therefore, we chose $\alpha_n = 0.21$ for NU in Figs. 4 and 5. In Fig. 4, we show the OP of FU as a function of IRS elements N and the Rician factor K, assuming there is no interference from the target sensing echo. This figure mainly demonstrates that the simulation results of OP exactly match the derived expression using the LT-based approach for FU in the high SNR regime. It can be observed that the OP improves with the increase in N without requiring additional Tx power. Also, OP improves as K increases for a fixed N. Further, by observing the slope of the OP curve for $N = 2$ at high SNR, the diversity order under the NOMA scheme is 2, which is consistent with our derived results.

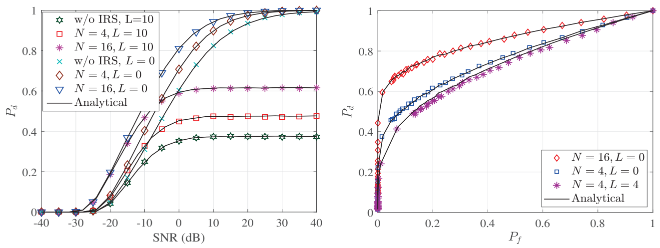

(a) (b)

Fig. 6: (a) PoD P_d vs SNR for different values of N and L, (b) ROC P_d vs P_f at $\mathrm{SNR}=0$ dB.

In Fig. 5, the OP as a function of SNR for various scenarios and for a fixed number of reflecting elements $N = 4$ is depicted. We observe that the NU experiences a better outage than the FU when the phase shifts of the IRS elements are randomly distributed. However, the OP of the FU improves significantly when the IRS phase shifts are optimized for the FU. For the optimal phase shifts at the IRS, the OP of the analytical curve derived from the CLT closely aligns with the simulated curve at low SNR (~ 10 dB), whereas the LT-based analytical curve accurately coincides with the simulated OP curve in the high SNR. In the presence of sensing echo interference, the OP tends to saturate in the high SNR regime. The asymptotic OP can be obtained by substituting $\lambda_f = \frac{\Lambda_f \sigma^2_{\zeta_f}}{(\alpha_f - \alpha_n \lambda_f)}$ into (20) and $\lambda_n = \max\left(\frac{\Lambda_f \sigma^2_{\zeta_n}}{(\alpha_f - \alpha_n \Lambda_f)}, \frac{\Lambda_n \sigma^2_{\zeta_n}}{\alpha_n}\right)$ into (23) for FU and NU, respectively. It can be observed that for the FU, the outage saturates at 10^{-1} under the random phase shifts, while for the optimal phase shifts, it is at 10^{-5}. A comparison with the OMA scheme demonstrates that the OP using OMA is better than that of NOMA for the NU case. We observe that for $\mathrm{SNR} > 7$ dB, the OP of FU with the NOMA scheme is better than the NU with the OMA scheme. For the FU case, the OP of NOMA always outperforms the OMA, while the slope of the OP in high SNR is the same for both OMA and NOMA schemes.

Fig. 6(a) shows the PoD as a function of transmit SNR. In this figure, we analyze the PoD of the target using the echo signal with and without IRS. The results demonstrate a significant enhancement in the PoD when the IRS is utilized, regardless of whether clutter is present or absent. Although the IRS is optimal for FU, it still enhances the PoD compared to scenarios with only the direct link (without the IRS). This indicates that integrating the IRS into the ISAC system offers substantial benefits for target detection. Further, in Fig. 6(b), we present the ROC P_d vs P_f for different numbers of reflecting elements (N) and clutter (L) at a fixed transmit $\mathrm{SNR} = 0$ dB. The area under the curve (AUC) of an ROC is used to evaluate the performance of the detector, with a higher AUC indicating a better detection capability. It can be observed from the figure that for a fixed value of $P_f = 0.2$, the P_d values for $N = 16$ and 4 are 0.78 and 0.6, respectively. This indicates that the sensing performance of the system improves with an increasing number of IRS elements.

VI. Conclusions

This paper analyzed the IRS-assisted ISAC system with the NOMA transmission scheme focusing on the OP under random and optimal phase shifts at the IRS while simultaneously performing the target detection at the ISAC transceiver. For the Rayleigh-Rician cascaded channel, we derived an LT-based exact statistic near low channel gain, which provides an accurate OP characterization in the high SNR regimes to overcome the limitation of inaccuracy using CLT-based approximation. Additionally, the paper investigates interference from sensing echoes and clutter, which impact communication performance. We also analyzed the sensing performance of the target in terms of PoD and ROC. The results demonstrate that optimal IRS phase shifts for the far user significantly enhance communication reliability by reducing OP. Also, the usage of IRS improves the target detection probability, although the phase shifts are not optimally designed for target sensing.

References

[1] A. S. Parihar *et al.*, "Performance analysis of NOMA-enabled active RIS-aided MIMO heterogeneous IoT networks with integrated sensing and communication," *IEEE Int. of Things J.*, vol. 11, no. 17, pp. 28 137–28 152, Sep. 2024.

[2] F. Liu *et al.*, "Integrated sensing and communications: Toward dual-functional wireless networks for 6G and beyond," *IEEE J. Sel. Areas in Commun.*, vol. 40, no. 6, pp. 1728–1767, Jun. 2022.

[3] X. Song *et al.*, "Joint transmit and reflective beamforming for IRS-assisted integrated sensing and communication," in *Proc. IEEE Wireless Commun. and Netw. Conf. (WCNC)*, Austin, TX, USA, 10-13 Apr. 2022, pp. 189–194.

[4] Z.-M. Jiang *et al.*, "Intelligent reflecting surface aided dual-function radar and communication system," *IEEE Sys. Journ.*, vol. 16, no. 1, pp. 475–486, Mar. 2022.

[5] C. Ouyang, Y. Liu, and H. Yang, "Performance of downlink and uplink integrated sensing and communications (ISAC) systems," *IEEE Wireless Commun. Letts.*, vol. 11, no. 9, pp. 1850–1854, Sep. 2022.

[6] X. Yue and Y. Liu, "Performance analysis of intelligent reflecting surface assisted NOMA networks," *IEEE Trans. Wireless Commun.*, vol. 21, no. 4, pp. 2623–2636, Apr. 2022.

[7] Wang *et al.*, "NOMA empowered integrated sensing and communication," *IEEE Commun. Letts.*, vol. 26, no. 3, pp. 677–681, 2022.

[8] J. Zuo *et al.*, "Exploiting NOMA and RIS in integrated sensing and communication," *IEEE Trans. Veh. Tech.*, vol. 72, no. 10, pp. 12 941–12 955, Oct. 2023.

[9] Y. Cheng *et al.*, "Downlink and uplink intelligent reflecting surface aided networks: NOMA and OMA," *IEEE Trans. Wireless Commun.*, vol. 20, no. 6, pp. 3988–4000, Jun. 2021.

[10] M. A. Richards *et al.*, *Fundamentals of radar signal processing*. McGraw-Hill New York, 2005, vol. 1.

[11] Q. Wu *et al.*, "Intelligent reflecting surface-aided wireless communications: A tutorial," *IEEE Trans. Commun.*, vol. 69, no. 5, pp. 3313–3351, May 2021.

[12] J. Proakis and M. Salehi, *Digital Communications, 5th edition*. McGraw-Hill Higher Education, 2008.

[13] Z. Ding, R. Schober, and H. V. Poor, "On the impact of phase shifting designs on IRS-NOMA," *IEEE Wireless Commun. Letts.*, vol. 9, no. 10, pp. 1596–1600, Oct. 2020.

[14] N. O'Donoughue and J. M. F. Moura, "On the product of independent complex Gaussians," *IEEE Trans. Sig. Process.*, vol. 60, no. 3, pp. 1050–1063, Mar. 2012.

[15] D. W. Lozier, "NIST digital library of mathematical functions," *Annals of Mathematics and Artificial Intelligence*, vol. 38, pp. 105–119, 2003.

[16] I. S. Gradshteyn and I. M. Ryzhik, *Table of integrals, series, and products*. Academic press, 2014.

[17] S. M. Kay, *Fundamentals of statistical processing, Volume 2: Detection theory*. Pearson Education India, 2009.